

Volumetric Data Exploration with Machine Learning- Aided Visualization in Neutron Science

Yawei Hui*

Computer Science and Mathematics Division, Oak Ridge National Laboratory, Oak Ridge, TN 37831

Yaohua Liu**

Quantum Condensed Matter Division, Oak Ridge National Laboratory, Oak Ridge, TN 37831

This manuscript has been authored by UT-Battelle, LLC under Contract No. DE-AC05-00OR22725 with the U.S. Department of Energy. The United States Government retains and the publisher, by accepting the article for publication, acknowledges that the United States Government retains a non-exclusive, paid-up, irrevocable, world-wide license to publish or reproduce the published form of this manuscript, or allow others to do so, for United States Government purposes. The Department of Energy will provide public access to these results of federally sponsored research in accordance with the DOE Public Access Plan (<http://energy.gov/downloads/doe-public-access-plan>).

Volumetric Data Exploration with Machine Learning-Aided Visualization in Neutron Science

Yawei Hui*

Computer Science and Mathematics Division, Oak Ridge National Laboratory, Oak Ridge, TN 37831

Yaohua Liu**

Quantum Condensed Matter Division, Oak Ridge National Laboratory, Oak Ridge, TN 37831

ABSTRACT

Recent advancements in neutron and x-ray sources, instrumentation and data collection modes have significantly increased the experimental data size (which could easily contain $\sim 10^8$ - 10^{10} points), so that conventional volumetric visualization approaches become inefficient for both still imaging and interactive OpenGL rendition in a 3-D setting. We introduce a new approach based on the unsupervised machine learning algorithm, Density-Based Spatial Clustering of Applications with Noise (DBSCAN), to efficiently analyze and visualize large volumetric datasets. Here we present two examples, including a single crystal diffuse scattering dataset and a neutron tomography dataset. We found that by using the intensity as the weight factor during clustering, the algorithm becomes very effective in de-noising and feature/boundary detection, and thus enables better visualization of the hierarchical internal structures of the scattering data.

Keywords: Scientific visualization, unsupervised learning and clustering, DBSCAN, volumetric dataset, neutron science.

Index Terms: • Human-centered computing~Scientific visualization • Computing methodologies~Cluster analysis

1 INTRODUCTION

It has been a long-term challenge to effectively visualize 3-D objects derived from large volumetric datasets in many scientific disciplines, industry domains and medical applications [1-3]. Most implemented techniques focus on the direct volume-rendering (DVR) algorithm which excels in its high sensitivity to the delicate structures of the 3-D objects at the expense of computational costs. For moderately sized datasets (typically $\sim 10^6$ - 10^7 data points) of simple density profiles, it is relatively easy to manipulate transfer functions (TF) [4, 5] used in DVR (e.g., threshold cut-off and segmented alpha ranges) so that independent features of the 3-D object and the boundaries between the signal and background noise can be well determined. However, when the complexity of the internal structures or simply the sizes of the datasets increase, it enters the domain of large datasets (typically $\sim 10^8$ - 10^{10} data points) and a simple scheme involving only TF manipulation can no longer work efficiently.

Here we propose a new visualization analysis approach that, beside the TF manipulation, takes accounts of spatial statistics of the data points. This approach enables one to explore fine structures in the sense of spatial clustering of 3-D objects. As a preliminary and yet crucial step in the visualization workflow, this analysis will play the roles of noise-filtering, feature-clustering with boundary

detection, and generating well-defined subsets of data for the final visualization.

Among several algorithms that we have tested (including kMeans, Independent Component Analysis, Principle Component Analysis, Blind Linear Unmixing, etc.), we found that the Density-Based Spatial Clustering of Applications with Noise (DBSCAN) [6] is very effective to accomplish the clustering tasks for our visualization analysis. Surprisingly, there are very limited applications of this algorithm for 3-D datasets so far [7-10]. Therefore, we have explored thoroughly, for the first time, this algorithm for its ability in detecting/identifying 3-D features and creating visualization from large datasets.

Two exemplary applications of our method have been presented with neutron datasets from a single crystal diffuse scattering experiment and a neutron tomography imaging experiment, acquired at the Spallation Neutron Source (SNS) and the High Flux Isotope Reactor (HFIR), respectively, at Oak Ridge National Laboratory (ORNL). Recent advancement in neutron sources, instrumentation and data collection modes have pushed the size of experimental datasets into the big data domain, which poses challenges for both still imaging and interactive OpenGL rendition in a 3-D setting. Interestingly, our work shows that, by using the intensity as the weight factor in the clustering process, DBSCAN enables one to spatially separate and extract interesting scattering features from the bulk data. A single feature or a combination of many of them could be chosen to create concise yet highly informative 2-D projections of the 3-D objects (i.e. still imaging), or to render 3-D OpenGL objects interactively so that one could explore the datasets in much more details by moving, rotating and zooming in/out around them.

In following sections, we will focus on the visualization analysis in Section 2, the applications of DBSCAN on neutron datasets in Section 3, some discussions and perspectives on future work in Section 4, and a brief conclusion in Section 5.

2 VISUALIZATION ANALYSIS

The goal of our visualization procedure is to explore and identify independent features for visualization and eliminate the noise at the same time, with as less user interference as possible. In this section, we will first introduce some specific characteristics of the neutron datasets and show the traditional DVR visualization via solely TF manipulation on these datasets. We then lay out the details of the DBSCAN-aided visualization analysis.

2.1 Characteristics of the 3-D Neutron Data

The first dataset was collected at the elastic diffuse scattering spectrometer beamline CORELLI at SNS on a sample of single-crystal calcium-stabilized zirconia of composition $Zr_{0.85}Ca_{0.15}O_{1.85}$ (CZO hereafter). The experimental data have been reduced into the sample's reciprocal space using Mantid [11, 12]. The reduced scattering dataset is saved as a 701 x 701 x 701 3-D matrix with

* huiy@ornl.gov, ** liuyh@ornl.gov

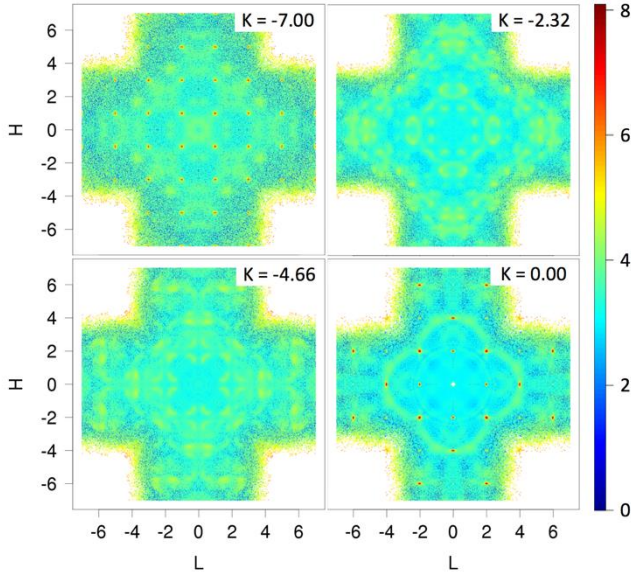


Figure 1: Exemplary 2-D cross-section images of the single crystal diffuse scattering data from calcium-stabilized zirconia of composition $Zr_{0.85}Ca_{0.15}O_{1.85}$. The 2D slices were cut perpendicular to the K axis in the sample's reciprocal space with a thickness of 0.02 rlu. Data are plotted with relative scattering intensity in the logarithmic scale. There are NaN entries representing no experimental data at corners in each image.

dimensions along the H, K and L axis of the reciprocal lattice. Figure 1 shows several exemplary 2-D slices cut perpendicular to the K axis. The intensity of CORELLI data typically spans a high dynamic range (~ 6 orders of difference in magnitude). There exist both Bragg peaks (strong and sharp spots seen in slices $K = -7$ and $K = 0$) and diffuse scattering (broad and weak features pervasive in all slices). All NaN values which represent no experimental data are pre-emptively removed from the visualization. These sliced images clearly show intricate structures existing in the 3-D dataset, which are of researchers' most interest to be visualized.

The second dataset was created from a tomographical reconstruction process on an Inconel 718 turbine blade (Turbine hereafter), imaged at the CG-1D cold neutron imaging prototype facility at HFIR of ORNL [2]. After the reconstruction, the Turbine dataset is saved as a $1997 \times 1997 \times 1997$ matrix with dimensions along the X, Y, Z axis of the 3-D real space. Figure 2 shows selected 2-D sliced images at different Z-positions. The noise can be seen in these images as both bulky background and filaments which are the relics of the tomography reconstruction. An efficient way to filter out these background noise before the 3D visualization is needed.

In both cases, the intensity of each data point has certain physical meaning. For the Turbine data, the intensity reflects the amplitude of the interaction potential between neutrons and the sample in the real space; while for the single crystal diffuse scattering data, the intensity is the 3D spatial Fourier transformation of the neutron-sample interaction potential.

2.2 Traditional DVR with TF Manipulation

A scrutiny on the intensity profile (e.g. a histogram of the intensity) along with intuition gained from 2-D cross-section images reveals that many interesting structures/features are often mingled together and mixed with the vast background of noise, therefore

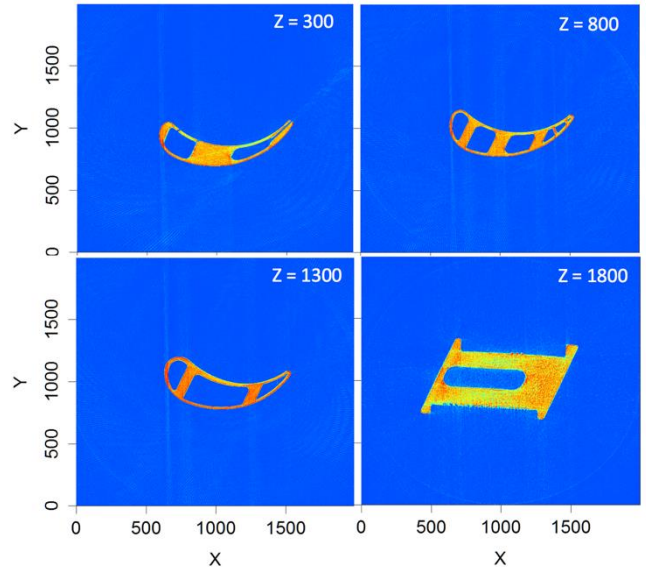


Figure 2: 2-D cross-section images along the Z-axis in the real space after the tomography reconstruction for an Inconel 718 turbine blade, imaged at the CG-1D cold neutron imaging prototype facility at HFIR of ORNL. The background noise can be clearly seen in these images.

investigating the intensity profile alone is not effective for feature detection and identification, as illustrated in Figure 3. We show in Figure 3(a) the histogram of intensity of the CZO dataset with several local extrema identified and in Figure 3b a scatterplot of the 3-D diffuse scattering image. For clarity, the visualization space is limited to a cuboid with dimensions of (301, 501, 301) along the axis of (H, K, L) in the reciprocal space.

The first extreme marked at "CUSP" in the histogram reflects the random fluctuation of the background noises in the 'empty' reciprocal space where the scattering signal from the sample and instrument is vanishingly small. Therefore, we set the cut-off intensity at "CUSP", which marks and removes 0.5% of the data points as "noise". For the rest of the "signal" data points, the dynamic range in their intensities spans more than 6 orders of magnitude and the total number of data points remains ~ 45 Million ($\sim 301 \times 501 \times 301$) in total. To avoid the overlapping problem in the 3-D scatterplot, we choose non-uniform "alpha" (i.e. transparency) in the TF, otherwise the scatterplot will simply manifest as a solid colored block. On the other hand, to visualize both the weak diffuse features and the strong "Bragg peaks" which reside at the opposite ends in the intensity profile, we divide the range of alpha at the value "THRESHOLD" into two segments. The first one covers the weak signals in the intensity range [CUSP, THRESHOLD] with the alpha values changing linearly from 0 to 1; the second keeps a constant alpha value (=1) for all points with intensities beyond THRESHOLD. Practically, it is of a trial-and-error matter to choose a proper value for THRESHOLD and it requires good understanding of the datasets. Even though some structured 3D diffuse scattering patterns show up in Figure 3(b), the patterns are overall vague and cloudy with noises, making it very difficult to characterize the morphological features.

2.3 DBSCAN-assisted DVR

In our new approach, before employing traditional DVR for 3-D visualization, we reduce the data via the unsupervised clustering

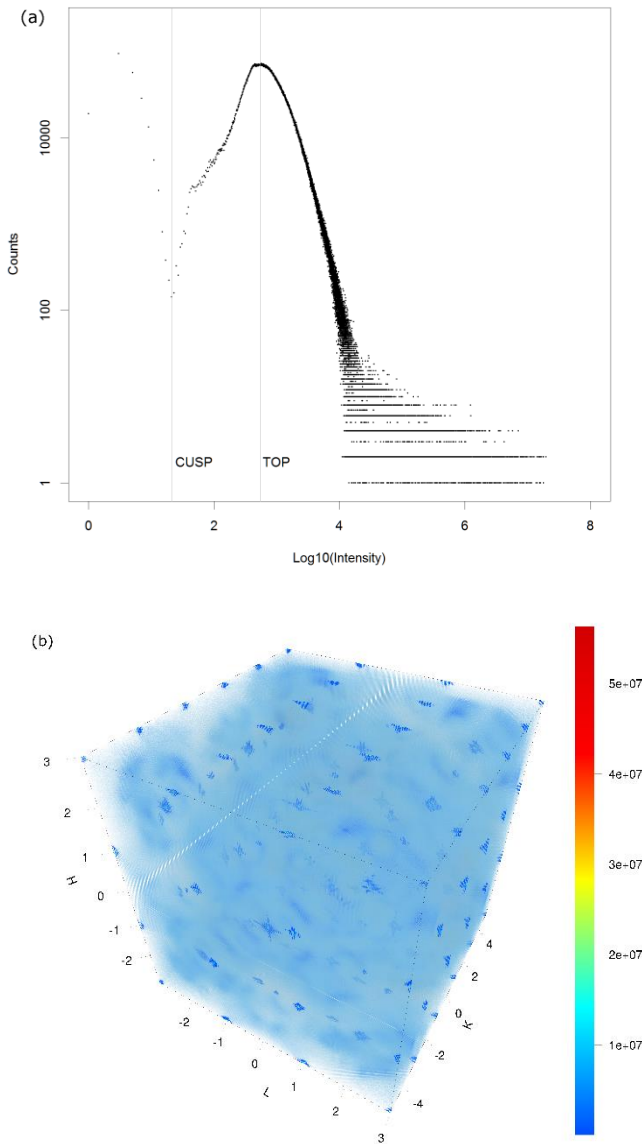


Figure 3: (a) Intensity histogram of the CZO dataset in a cuboid with dimensions (301, 501, 301) along (H, K, L) axes. (b) 3-D still image of the CZO dataset obtained solely by TF segmentation. Data are shown on the linear scale of intensities with noises removed below “CUSP” and a segmented TF divided at $\text{THRESHOLD} = 50 \cdot \text{TOP}$.

algorithm DBSCAN to remove noise points by default and to facilitate the features and object boundaries detection.

The general form of DBSCAN takes two parameters in the clustering procedure: ϵ - the maximum distance between two points for them to reside in the same neighborhood; and minPts - the minimum number of points required to form a dense region. The distance between two points is usually defined in the Euclidean metric. In the neutron datasets discussed here, coordinates of the data points are taken as the uniformly distributed voxel indices which scale linearly with the physical positions of data points in either the reciprocal space for the diffuse scattering dataset, or the

real space for the tomography dataset. The calculation of the parameter ϵ would then be greatly simplified. For a Cartesian coordinate system, if considering only the smallest “ ϵ -neighborhood” of an arbitrary point, we can set ϵ between $[1, \sqrt{2}]$ which will include only the six first nearest neighbors. To expand the ϵ -neighborhood, we can choose the value of ϵ in $[\sqrt{2}, \sqrt{3}]$ to include the twelve second nearest neighbors, and so on. In the following visualization and discussion, we keep ϵ fixed at 1.7 so that only the 18 nearest neighbors (1st and 2nd) are taken into the calculation of the density for local clustering.

The most critical adaptation to apply DBSCAN on our neutron datasets is to use the intensity as a measure of weight in calculating the second DBSCAN parameter – minPts. As mentioned above, the intensity of neutron scattering data is of physical significance, however the traditional DVR algorithm doesn’t take it into account when designing the TF. It’s obvious that the diffuse scattering patterns shown in both 2-D (Figure 1) and 3-D images (Figure 3(b)) are as much spatially correlated as photometrically. To utilize both information, i.e., the intensity and spatial location, we dictate the algorithm to calculate minPts with varying weights so that for each data point, its contribution to weighted-minPts is proportional to its intensity. By doing so, the DBSCAN algorithm becomes very effective in de-noising and feature/boundary detection for neutron scattering data. For example, for the single crystal diffuse scattering dataset, with a proper weighted-minPts value, one can detect both the Bragg peaks (sharp spots with a few high intensity points) and the diffuse scattering patterns (broad features with many low intensity points), and label them in different clusters provided sufficient spatial separations, as shown in the next section.

Among many controls/tweaks one could apply in the clustering process in order to tailor DBSCAN to a certain need, we utilize its native ability of distinguishing in a cluster the “core” points from its boundary points. This feature will play a critical role of intelligently reducing the size of the dataset and making it practical to interactively manipulate the 3-D object created from the Turbine dataset.

3 APPLICATION ON NEUTRON DATA

Without loss of generality, we use 3-D scatterplots for visualization after the DBSCAN clustering analysis. These scatterplots use a simple TF which maps the relative intensities of points in a cluster to a continuous alpha range in $[0, 1]$.

3.1 Feature extraction in single crystal diffuse scattering

Figure 4 shows the results from the DBSCAN clustering and the final visualization of the single crystal diffuse scattering dataset. Specifically, Figure 4(a) shows a 3-D still image of the CZO dataset which includes all clusters identified by DBSCAN using $\epsilon = 1.7$ and weighted minPts = 70. With this set of parameters, DBSCAN identifies 668 clusters in total, which covers 6.5% of the total ~45M data points. In another word, 93.5% of the data points are identified as noise (or NaN), and will not be used for visualization. In comparison to traditional DVR result shown in Figure 3(b), DBSCAN has removed the cloudy background so that the spatially isolated structures stand out, which is of tremendous help on visualizing morphological features of the diffuse scattering patterns in the 3D reciprocal space.

More importantly, DBSCAN provides an easy way to extract distinct 3D diffuse scattering features from the volumetric data and make it possible to examine each individual diffuse scattering feature in detail independently. For examples, Figure 4(b) and (c) show the first prominent group of two clusters and the second prominent group of eight clusters, respectively. Detailed close-up could be easily achieved by simply selecting the desired cluster for visualization and such an example is given in Figure 5. The top two

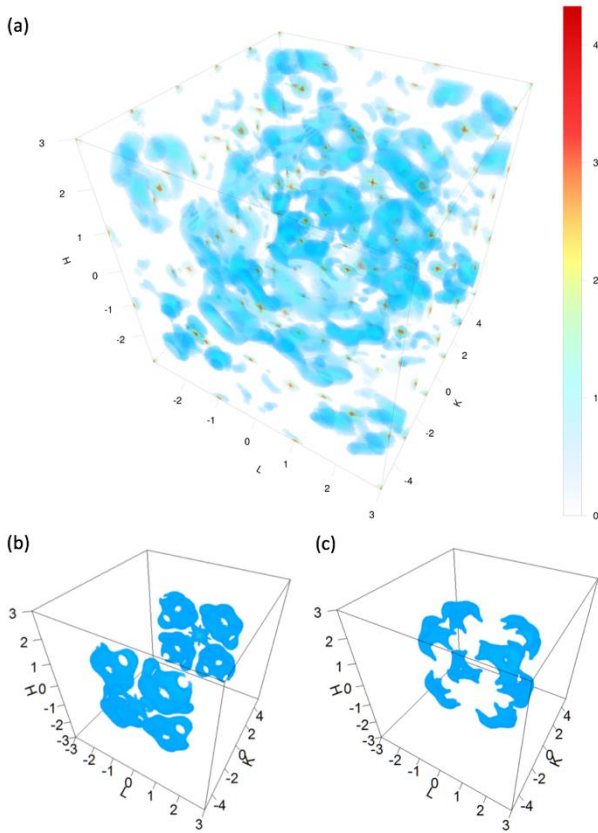


Figure 4: (a) A 3-D still image of the CZO dataset with all clusters identified by DBSCAN using $\epsilon = 1.7$ and weighted minPts = 70. (b, c) 3-D scatterplots of clusters grouped per symmetry – (b) the most prominent two clusters; and (c) the next group of eight prominent clusters. Data are shown on the logarithmic scale of relative intensities.

panels present scatterplots of the most prominent two clusters identified in Figure 4(b) in different spatial perspectives. The bottom two panels show the same object but plotted in isosurfaces which reveal finer internal structures of the cluster.

3.2 Interactive visualization of neutron tomography

Besides usual tasks like denoising, the neutron tomography dataset brings another challenge with its gigantic size to the visualization analysis. In our case, the raw Turbine dataset contains 8×10^9 data points in total and its intensity histogram is shown in Figure 6. Similar to the last example in Section 3.1, the data points with low intensities ($< 10^{-3}$) are mostly from the background noise and can be filtered out without losing useful information. Applying this filter reduces the total points to a still large number of 3.4×10^8 .

Popular visualization packages (such as ParaView, Tomviz) couldn't handle such large datasets in their original format. Although some professional products like VGStudio can deal with this big data problem, it is impractical for neutron scientists and general facility users to use them daily for quick exploration of their datasets. Besides the high cost of the license and maintenance associated with these specialty software, the learning curve is usually so high that a dedicated staff member must devote a significant amount of time and effort to master the massive set of

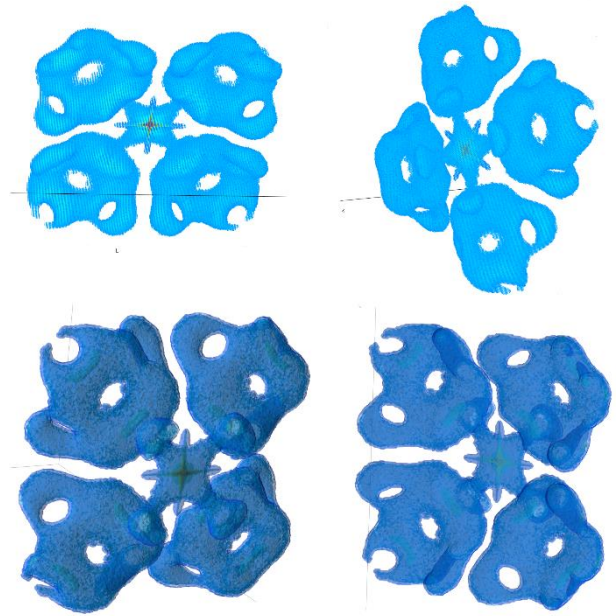


Figure 5: Top panels - Scatterplots of one of the most prominent cluster identified in Figure 4(b) in different spatial perspectives; Bottom panels – isosurfaces of the same object revealing finer internal structures.

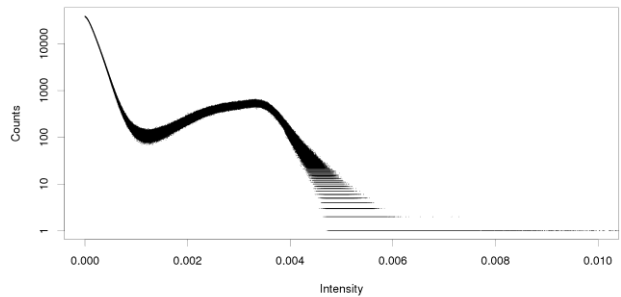


Figure 6: Intensity histogram of the Turbine dataset. Negative intensity data points are not shown in the histogram.

functionalities provided in these products.

To find a simple yet efficient way to deal with the big data problem in visualizing the tomography datasets, we found that the application of DBSCAN is easy to implement and can significantly improve the performance of the visualization, as demonstrated in rendering the 3-D OpenGL object of the turbine blade interactively (see screenshots in Figure 7). The general procedure of applying DBSCAN to the tomography dataset is similar to that used in the feature detection in Section 3.1. One critical deviation is that we apply the DBSCAN twice in the visualization analysis. The first DBSCAN identifies the bulk volume of the turbine blade as a single cluster and, at the same time, removes all the data points outside the bulk volume as noise. Comparing to traditional denoising the

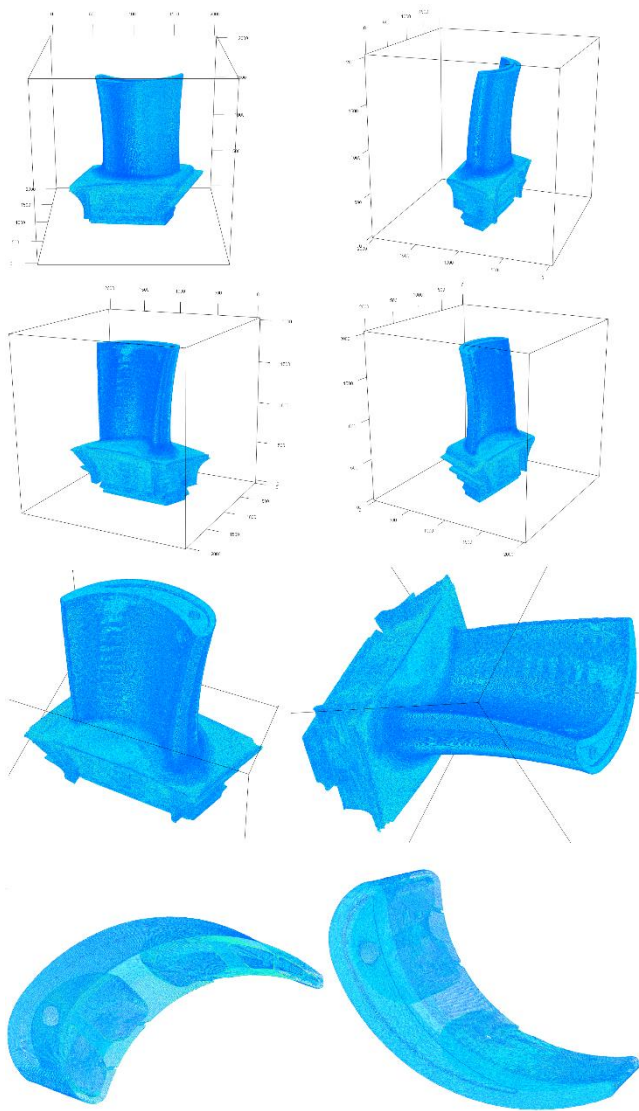


Figure 7: Screenshots of the 3-D OpenGL rendition of the Turbine dataset. The series show the capability of manipulating this object in several interactive modes including rotating, moving and zooming in/out with a general purpose personal laptop. The bottom two panels show a regional view of the top quarter of the turbine blade, which clearly reveals the internal structure of the 3-D object. Relative intensities are plotted here with the grid coordinates in the real space.

procedure which sets a subjective intensity value as the cutting threshold and thus may risk feature losses, DBSCAN takes advantages of the spatial statistics of the imaged object to define its boundary.

After the first DBSCAN clustering, the number of points representing the de-noised 3-D object is reduced to 1.1×10^8 from 3.4×10^8 . However, it's still too big to create an interactive visualization with such a large dataset. One way to solve this problem is to only render the surface of the object so that one can interactively visualize the 3D neutron tomography even with a moderately-equipped hardware.

To get the surface data points, we perform a second DBSCAN clustering on the original dataset but explicitly demand it to drop all the boundary points so that the resulting cluster contains only the points confined within the bulk volume of the turbine blade. By subtracting all points in this “peeled-off” cluster from those points in the cluster generated in the first DBSCAN, we get a “thin skin” (pure boundary) of the 3-D object. The final number of points to visualize is dramatically reduced to 3.2×10^7 , or by a factor of 10 comparing to the original. This double-DBSCAN approach raises the efficiency of the interactive visualization so much that the entire 3-D object could be rendered on a personal laptop with a generic integrated graphics card, as shown in the screenshots in Figure 7.

4 DISCUSSION

4.1 Involvement of HPC

In our work, we have resorted to the computational resources provided by the Rhea cluster at Oak Ridge Leadership Computing Facility (OLCF) at ORNL. All still images presenting full datasets such as in Figs. 3(b) and 4(a) are created on one of the Rhea’s GPU nodes which provides two NVidia K80 GPUs with 1TB memory. Besides these tasks, other computationally intensive jobs such as the DBSCAN clustering on large datasets are also carried out on the Rhea nodes. As an initiative focusing on the viability of using DBSCAN to help on efficiently visualizing volumetric datasets, this work hasn’t been exploring any potential performance gains from a distributed computing scheme. For example, all the DBSCAN clustering processes have been carried out with the R function provided in the “dbscan” package. Apparently, if replaced by a parallel implementation of the DBSCAN using MPI, the execution time of this algorithm (typically around 20 to 30 minutes for $\sim 10^8$ data points) will be much reduced (potentially linearly downscaled with requested computational resources).

Another call to distributed computing (which is the forte of the HPC platforms at OLCF) comes from the heavily burdened I/O system on the Rhea node. By using the HDF5 format to store the volumetric datasets used in this work, we have significantly reduced the READ_IN time (from disks to memory) by an order of magnitude (comparing to loading and combining tomography images in their TIFF format). However, it still takes 19 mins to read the 59 GB Turbine dataset into the memory. In future development, we could use the parallel HDF5 API in the I/O design to mitigate this performance bottleneck.

4.2 Expanding DBSCAN’s applications in neutron science

4.2.1 Diffuse scattering research

Analyzing volumetric single-crystal diffuse scattering data remains a high technique hurdle due to the large size of the datasets (typically $\sim 10^9$ data points per dataset). The conventional approaches, such as 2D slicing, are tedious and error-prone to explore the vast volume in the 3D reciprocal space to identify characteristic features. Derived from our visualization analysis, intensity-weighted DBSCAN is found to be very effective in extracting distinguishable 3D features in diffuse scattering datasets. Given common geometrical characteristics exist in these features, a database of such features could be built upon the identification and curation of sufficiently ample examples. As a 3D visual library, the database could facilitate researchers to quickly get insight into underlying microstructural origins of the diffuse scattering features observed in their experiments. More importantly, it could potentially enable scientists to better correlate physical properties and local deviations from the average structure, the latter of which is the cause of diffuse scattering, so that functional materials can be classified by their intrinsic local structures.

4.2.2 Neutron experiment monitoring

Further improvement on performance of our visualization analysis with the help of HPC resources at OLCF (discussed shortly in Section 4.1) could enable the analysis and visualization of real-time streaming data collected at multiple SNS/HFIR beamlines. By using such tools during experiments, users could identify weak scattering features at an early stage of the experiment and better plan the following steps so that the neutron beam time could be used more efficiently.

As a joint effort between OLCF and SNS, we have been working on the initial stage of integrating DBSCAN-aided visualization analysis into the Bellerophon Environment for Material Analysis (BEAM), a workflow management system developed at ORNL [13], which will connect the neutron data sources with the HPC at OLCF to speed up the analysis and visualization.

4.2.3 Tomography Imaging

As a visualization analysis approach, intensity-weighted DBSCAN could be generalized to applications on tomography imaging illuminated by not only neutron but also other particle sources (X-ray and electron, etc.). In this work, we have demonstrated the capability of this new approach with a simple example of interactive 3-D rendition. This method could be extended to effectively detect 3-D defects (e.g. cavities, cracks), 2-D or 3-D heterogeneous interfaces inside the imaged objects. All the analysis and visualization could be carried out onsite along with the ongoing imaging process.

5 CONCLUSION

We have investigated DBSCAN for neutron scattering data analysis and visualization with two examples, including feature extraction in a single crystal diffuse scattering dataset and interactive 3-D visualization of neutron tomography dataset. In both cases, the intensity at each data point is of physical significance and can be used in DBSCAN clustering as the weight-factor to evaluate the input parameter minPts. By doing so, we are using both the photometric and spatial information of the scattering data in the visualization analysis, and it turns out to be a very effective approach to analyze and visualize large volumetric neutron datasets.

ACKNOWLEDGEMENT

We first thank Dr. Lin Jiao at the Neutron Data Analysis & Visualization Division (ORNL) for providing the Turbine dataset used in this article, and Dr. Jean-Christophe Bilheux at the Neutron Data Analysis & Visualization Division (ORNL) for discussions and illustrations of functionalities of tomography visualization in VGStudio. We also thank our colleagues, Mr. Eric Lingerfelt at the Computer Science & Mathematics Division (ORNL) and Dr. Christina Hoffmann at the Chemical & Engineering Materials Division (ORNL) for insightful discussions. This research used resources of the Oak Ridge Leadership Computing Facility at the Oak Ridge National Laboratory, which is supported by the Office of Science of the U.S. Department of Energy under Contract No. DE-AC05-00OR22725. Research conducted at ORNL's Spallation Neutron Source and the High Flux Isotope Reactor was sponsored by the Scientific User Facilities Division, Office of Basic Energy Sciences, U.S. Department of Energy.

REFERENCES

[1] O. Kreylos, G. H. Weber, E. W. Bethel, J. M. Shalf, B. Hamann and K. I. Joy. Remote Interactive Direct Volume Rendering of AMR Data, *Tech. Rep.*, LBNL 49954, Lawrence Berkeley National Laboratory (2002).

<http://vis.lbl.gov/Publications/2002/LBNL-49954-AMRVVolumeRendering.pdf>

[2] T. R. Watkins, H. Z. Bilheux, K. An, E. A. Payzant, R. R. Dehoff, C. E. Duty, W. H. Peter, C. A. Blue and C. A. Brice. Neutron characterization for additive manufacturing. *Advanced Materials & Processes*, 171, 3, 23-27 (2013). <https://neutrons.ornl.gov/sites/default/files/AMP-17103p23.pdf>

[3] Q. Zhang, R. Eagleson and T. M. Peters. Volume Visualization: A Technical Overview with a Focus on Medical Applications. *Journal of Digital Imaging*, 24(4), 640 (2011). <http://doi.org/10.1007/s10278-010-9321-6>

[4] T. Peters. The physics of volume rendering. *Eur. J. Phys.*, 35, 065028 (2014). <https://doi.org/10.1088/0143-0807/35/6/065028>

[5] P. Ljung, J. Krüger, E. Groller, M. Hadwiger, C. D. Hansen and A. Ynnerman. State of the Art in Transfer Functions for Direct Volume Rendering. *Computer Graphics Forum*, 35: 669–691 (2016). doi:[10.1111/cgf.12934](https://doi.org/10.1111/cgf.12934)

[6] M. Ester, H.-P. Kriegel, J. Sander and X. Xu. A density-based algorithm for discovering clusters a density-based algorithm for discovering clusters in large spatial databases with noise. In *Proceedings of the Second International Conference on Knowledge Discovery and Data Mining (KDD'96)*, Evangelos Simoudis, Jiawei Han, and Usama Fayyad (Eds.). AAAI Press 226-231 (1996). doi: [10.1.1.121.9220](https://doi.org/10.1.1.121.9220)

[7] D. Piper, K. Schiecke, H. Witte and L. Leistritz. Comparative study of methods for solving the correspondence problem in EMD applications. *Current Directions in Biomedical Engineering*, 2(1), pp. 225-228 (2016). <https://doi.org/10.1515/cdbme-2016-0050>

[8] B. Gault, M. P. Moody, J. M. Cairney and S. P. Ringer. Atom Probe Microscopy. *Springer Series in Materials Science* 160, Springer, 2012, Chapt 8, 261 (2012). doi: [10.1007/978-1-4614-3436-8](https://doi.org/10.1007/978-1-4614-3436-8)

[9] S. Riggi, et al. Muon tomography imaging algorithms for nuclear threat detection inside large volume containers with the Muon Portal detector. *Nucl. Instrum. Meth.*, A728, 59-68 (2013). <https://doi.org/10.1016/j.nima.2013.06.040>

[10] T. N. Tran, et al. A density-based segmentation for 3D images, an application for X-ray micro-tomography. *Anal. Chim. Acta.*, 725:14-21 (2012). doi: [10.1016/j.aca.2012.03.008](https://doi.org/10.1016/j.aca.2012.03.008)

[11] O. Arnold, et al., Mantid — Data analysis and visualization package for neutron scattering and μ SR experiments, *Nuclear Instruments and Methods*, A764: 156-166 (2014). <http://dx.doi.org/10.1016/j.nima.2014.07.029>

[12] T. M. Michels-Clark, A. T. Savici, V. E. Lynch, X. P. Wang and C. M. Hoffmann. Expanding Lorentz and spectrum corrections to large volumes of reciprocal space for single-crystal time-of-flight neutron diffraction. *J. Appl. Cryst.*, 49(2): 497-506 (2016). <https://doi.org/10.1107/S1600576716001369>

[13] E. J. Lingerfelt, A. Belianinov, E. Endeve, O. Ovchinnikov, S. Somnath, J. M. Borreguero, N. Grodowitz, B. Park, R. K. Archibald, C. T. Symons, S. V. Kalinin, O. E. B. Messer, M. Shankar and S. Jesse. BEAM: A Computational Workflow System for Managing and Modeling Material Characterization Data in HPC Environments. International Conference on Computational Science 2016, *Procedia Computer Science.*, 80: 2276-2280 (2016). <https://doi.org/10.1016/j.procs.2016.05.410>